A Survey on Ageing Mechanisms in II and III-Generation PV Modules: Accurate Matrix-Method Based Energy Prediction Through Short-Term Performance Measures

P. Visconti*‡, R. de Fazio*, D. Cafagna*, R. Velazquez ** and A. Lay-Ekuakille*

*Department of Innovation Engineering, University of Salento, 73100, Lecce, Italy

** Universidad Panamericana, Facultad de Ingeniería, Aguascalientes, 20290, Mexico

(paolo.visconti@unisalento.it, roberto.defazio@unisalento.it, donato.cafagna@unisalento.it, rvelazquez@up.edu.mx, aime.lay.ekuakille@unisalento.it)

‡Corresponding Author; P. Visconti, Street for Monteroni, Ecotekne University Campus, Tel: +39 0832 297335, ZIP Code 73100, Lecce, Italy, paolo.visconti@unisalento.it

Received: 18.01.2021 Accepted:22.02.2021

Abstract- Solar energy utilization has been triggered by advances in new technology to reduce the cost of photovoltaic (PV) panels with an increase of efficiency. To improve the energy production quality, it is necessary to undergo the PV panels to characterization both in the indoor and outdoor scenarios; these latter characterizations generally require all seasons-based measurements. Therefore, it is essential to find models for characterizing PV panels in terms of energy production but also production and operating mode tolerance. The paper illustrates the findings of global research dedicated to PV panels ageing and their impact on energy production in the years. At first, an in-depth analysis of the ageing mechanisms affecting II and III generations' PV panels has been presented when exposed to atmospheric agents. Afterwards, the PV panels' characterization, conducted in a short time (i.e. a total of seven days), has been reported, performing outdoor measurements in conjunction with an electronic calibrator able to measure currents and voltages. The MPPT (Maximum Power Point Tracker) device is the core instrumentation of the employed measurement system. Obtained results are convincing since they have been compared with simultaneous measurements of PV panels located in the same place.

Keywords- Photovoltaic panels, energy prediction, sensors, maximum power point tracker, measurement system.

1. Introduction

Solar energy is the primary source for the generation of electrical power in terrestrial and space applications. The conversion efficiency is the main parameter for determining the performances of these devices. In the years, solar technology's evolution continuously increases conversion efficiency, reaching peaks of 40% for multi-junction solar cells [1-3]. However, the exposure to the environmental agents induces deterioration phenomena during their expected lifetime (20–25 years). The manufacturers usually declare a reduction of nominal power within 10% in the first 10–12 years and up to 20% after 20–25 years of operation [4]. These degradations are ascribable to several agents, such as UV radiation, high-temperature, moisture infiltration, and mechanical stress, which induce PV damage. These phenomena affect the PV panel's operation, gradually decreasing its electrical performances in terms of output power and conversion efficiency [5]. The PV manufactured and scientific community carries out enormous efforts to determine reliable and accurate models to predict performance degradation over time due to the plant's operative conditions to schedule maintenance and substitution operation. Several research works present in the scientific literature propose parametric laws to estimate the maximum electrical power degradation. In [6], M. Boussaid et al. proposed a modified Weibul model to determine the average lifetime of photovoltaic panels placed in the California desert, resulting in about 30 years; a genetic algorithm has been employed to determine the parameters model. Similarly, B. Nehme et al. have developed a mathematical model to simulate PV panel efficiency over

time, modelling the degradation modes, viz potential-induced degradation, light-induced degradation (LID) and UV.light degradation [7]. The obtained model has been employed to simulate the variation of efficiency overtime for a module constituted by two strings of 12 cells. In [8], the authors proposed a novel method for calculating the PV panel's degradation, estimating the modules series resistance increment. This last is calculated through the error in evaluating the maximum power point position, comparing the real data with the diode model. S. Lindig et al. have applied three statistic models, namely simple linear regression (SLR), classical seasonal-decomposition, seasonal- and trend-decomposition using Loess (STL), Holt–Winters exponential smoothing and autoregressive integrated moving average (ARIMA), to calculate the performance loss of two PV plants [9]. Obtained results demonstrated that the STL and ARIMA models show higher accuracy, but the first one is featured by a more straightforward implementation.

The remainder of the manuscript is structured as described below: section 2 reports the fundamental concepts of PV panels, related equations and parameters, which are essential to introduce the carried out experimental activities. Afterwards, two literature survey sections are reported; the first one presents an in-depth overview of ageing mechanisms affecting II and III generation PV panels. The latter discusses the different methods for forecasting the PV panels' solar energy, focusing on matrix and MotherPV methods. Section 5 describes the experimental setup used to calibrate the proposed matrix method. Finally, the experimental results and related discussions concerning power predictions are reported for different PV panels (CdTe and CIGS) technologies, comparing them with our database obtained collecting data over ten years.

2. Basic concepts of PV cells and related parameters

In this section, the fundamental concepts of PV panels, related parameters and equations are reported, fundamental to better understand the literature overview and carried out experimental activities. It is known that I-V is the most important characteristic of PV panel, allowing a direct knowledge of its operating mode and utilization (Fig. 1); from it, we can indirectly derive the open-circuit voltage (V_{oc}) supplied by the solar cell and the dark saturation current (I_0). V_{oc} is the maximum voltage that the panel is able to provide without any output load (zero current condition). By setting the net current equal to zero in the following solar cell equation [10], V_{oc} is obtained as:

$$V_{oc} = \frac{k_B T}{q} \ln\left(1 + \frac{I_{ph}}{I_0}\right) \quad (1)$$

The dark saturation current is derived by means of similar reasoning in terms of the photo-generated current I_{ph}, since it can be compared to the black-body photon flux at the cell temperature T_C, hence:

$$I_0 = Aqf_0 \Phi(E_g, T_a) \quad (2)$$

in which the coefficient f_0 has been included to determine correctly the total area f_0A exposed to the ambient photon flux, E_g is the energy gap, T_a the ambient temperature, Φ is the photon flux and q the charge. Dealing with PV panels and cells, if the PV cell provides a maximum power value (P_{max}) to which the voltage V_m and current I_m values correspond, then by using the I_{sc} (short circuit current) and V_{oc}, the fill factor (FF) parameter is defined as:

$$FF = \frac{I_m V_m}{I_{sc} V_{oc}} = \frac{P_{max}}{I_{sc} V_{oc}} \quad (3)$$

The optimal value of FF parameter relative to a solar cell with ideal electrical behaviour is described with subscript "zero" and cannot be calculated analytically; it can be demonstrated that the FF_0 value depends only upon the following ratio:

$$v_{oc} = \frac{V_{oc}}{k_B T} \quad (4)$$

$$FF_0 = \frac{v_{oc} - \ln(v_{oc} + 0.72)}{V_{oc} + 1} \quad (5)$$

The FF_0 parameter is determined by the approximate relationship:

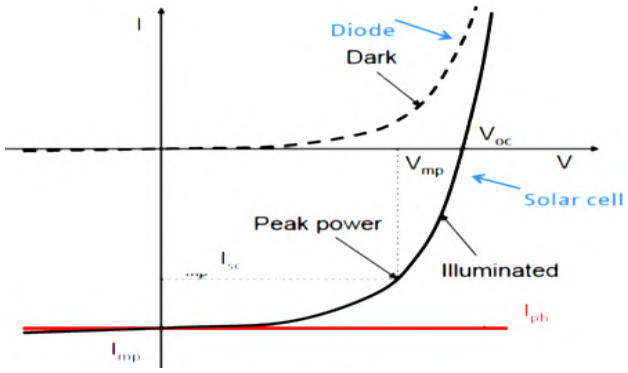

Fig. 1. Principle of super-position within I-V characteristics equated to a p-n junction working in dark and light (illuminated) conditions.

FF's impact is of great interest in the efficiency and yield of the PV cells/panels because it contains, in its diverse formulations, the maximum power P_{max} [11], and both main electrical parameters, namely V_{oc} and I_{sc}. From Eq. (3), it is:

$$FF = \frac{I_m V_m}{I_{sc} V_{oc}} = \frac{P_{\max}}{I_{sc} V_{oc}} = \frac{P_{\max}}{P_{th}} = \frac{P_m}{P_{th}} \Rightarrow P_{\max} = FF \cdot P_{th} \quad (6)$$

Having set according to Figs. 1 and 2, I_m and V_m respectively the maximum current and maximum voltage corresponding to the maximum power point (P_{max}). P_{th} is the theoretical power delivered by the PV panel. Now we can understand the correlation between FF and efficiency in its diverse formulation [12], that is:

$$\eta = \frac{P_{output}}{P_{input}} \Rightarrow \eta_{\max} = \frac{P_{\max}}{P_{input}} = \frac{FF \cdot P_{th}}{P_{input}} \quad (7)$$

Given the radiance *G* and area *A* of PV panel, it is obtained:

$$P_{input} = G \cdot A \quad (8)$$

The Eq. (8) leads to the following equation (9):

$$\eta_{\max} = \frac{FF \cdot P_{th}}{G \cdot A} \quad (9)$$

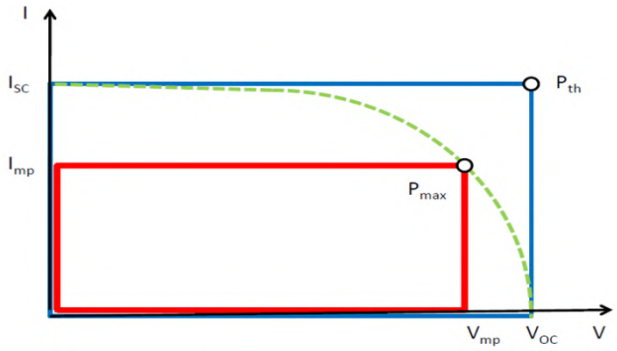

Fig. 2. Fill factor and I-V characteristic.

Eq. (9) is very helpful in testing and characterizing PV panels, even if it is done, as the main scope of present work, in a short time. It is also helpful to know that a good value of FF is in general greater than 0.75 and excellent panels possess a value of FF around 0.85 that is associated with a narrow interval of tolerance related to performance variations [13,14]. However, solar power and irradiance are featured by an intrinsic variability, related to changes in weather conditions (i.e. sky image, cloud cover, precipitation, sunshine duration and air pressure parameters), affecting quality and stability of the power produced by the solar plant [15]. The availability of accurate forecasting models is fundamental for the optimal modeling and scheduling solar photovoltaic power plants. The autoregressive integrated moving average model is usually employed for solar power forecasting, considering solar power, solar irradiance and air temperature the main parameters, covering a forecasting time horizon from few hours to days. Also, in [16], the authors employed empirical models and different machine learning algorithms to estimate the global solar radiation in different climatic zones of China. M. Afzaal *et al.* analyzed different probability distribution functions (in particular, the Weibull probabilistic model) for characterization of solar irradiance patterns [17]. Results compared with those of Beta model, certify model validity allowing to estimate solar irradiance and, thus, PV panel power generation in the following years.

The solar cells are classified into four categories, called generations, depending on constructive technology and materials. The first generation includes cells based on monocrystalline and polycrystalline silicon; the second generation cells rely on thin-film technology, like amorphous silicon, CdTe, CIS and CIGS. The third-generation cells comprise solution based on no-semiconductor materials, including organic solar cells (OPV), dye-sensitized solar cells (DSSC), quantum dot (QD) cells, perovskite cells, etc. The fourth-generation includes emerging PV technologies, like the hybrid in-organic crystals with a polymer matrix. Further details about the PV panels classification are provided in the following sub-section 3.1.

3. Ageing Processes and Performance Loss in II and III Generation PV Panels

In this section, we describe the main ageing processes affecting the PV panels of the second and third generation, resulting in the deterioration of the cells' overall performances, thus reducing the conversion efficiency of the harvesting system [18].

3.1. Classification of II and III Generation PV Panels

The second generation of PV panels includes modules based on thin-film technology of monocrystalline semiconductors, such as hydrogenated amorphous silicon (a-Si:H), indium copper diselenide (CIS), cadmium telluride (CdTe) (Fig. 3a), indium copper gallium diselenide (CIGS) (Fig. 3b), and gallium arsenide (GaAs), deposited on a thin and flexible substrate which are widely spread on the market and used in several applications, since their flexibility enable the integration of solar harvesters in everyday objects (i.e. portable devices, remote sensor nodes, self-charging power supply systems, wearable applications etc.). However, these PV technologies are featured by lower costs than those of the first generation, but lower conversion efficiency compared to bulk technologies [19, 20]. Specifically, the thin-film technology offers several potentialities to reduce production costs due to the material savings and the manufacturing process's scalability, suitable for the series production. For instance, CIGS technology can reach relatively high conversion efficiencies up to 22.6% [21 - 23], comparable to commercial crystalline silicon cells. The GaAs technology represents the most interesting from the point of view of conversion efficiency, overcoming the 30-35%. However, the high production cost and material lack limit the applicability of this technology, currently used for space applications, where low weight and dimensions are required.

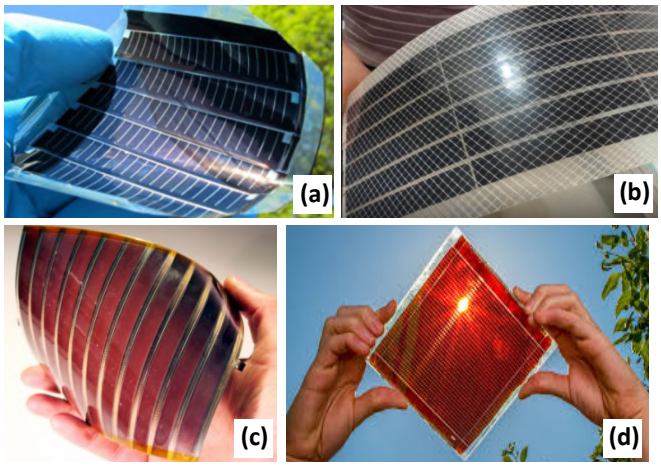

Fig. 3. Fully monolithically integrated flexible CdTe solar module (a); flexible CIGS module for outdoor applications (b); flexible DSSC (c), and Perovskite solar cells (d).

The technologies belonging to third-generation PV cells are the following: Organic Photovoltaics (OPV), Dye-Sensitized Solar Cells (DSSCs) (Fig. 3c), Zinc Tin Sulphide (CZTS), Perovskite solar cells (PSC) (Fig. 3d), and quantum dot solar cells [24, 25]. These technologies share a production process requiring the deposition of active materials in the form of liquid solutions, deposited on a plastic substrate between two transparent electrodes (e.g., thin metallic layers, ITO-Indium Tin Oxide, etc.) to collect the photo-generated current. Several research works deal with the development of solar paints able to substitute the conventional PV cells, given their enormous potentialities ascribable to the productive process's scalability, high flexibility, and low cost. The heterojunction cells can be manufactured with the roll-to-roll deposition printing

technology, allowing rapid and simple deposition of polymeric films on a wide area, thus eliminating the cleanroom's costs. However, the OPVs obtain lower conversion efficiency than the second generation PV panels, mainly due to the difference in exciton splitting between organic and inorganic materials and the shorter exciton lifetime in organic solar cells. DSSCs and quantum dot solar cells are strongly attracting the scientific community's attention, given the recent progress aimed to optimize their conversion efficiency, reaching values higher than 10%, thanks to the use of quantum dots and nanoporous materials, allowing to enlarge the cell's absorption spectrum up to 60% [26, 27]. The perovskite PV cells, since the introduction, have rapidly reached very high conversion efficiencies (>22%) [28]. However, this technology suffers from poor uniformity of the manufacturing process, making the scaling up of these devices very difficult. A significant issue of perovskite cells concerns their environmental impact since their lead content could contaminate water sources if a proper encapsulation isn't added. The multi-junction solar cells also belong to third-generation solar devices; they are designed to collect energy on a wide range of wavelengths, from the near-UV to mid-IR. [29]. This capability is obtained by combining multiple semiconductor junctions (e.g. 2, 3, or 4) to maximize the conversion efficiency. Currently, III-V $GaAs_{1-x}Bi_x$ alloys are widely studied for excellent properties like charge carriers mobility, energy gap and doping concentration, suitable to get high conversion efficiency.

3.2. Degradation Effects of the II Generation PV Panels

The PV cells are subjected to performance degradation due to their deterioration over time [30 - 33]. The proper understanding of the PV panels deterioration mechanisms is essential for determining the solar plant's lifetime and forecasting its performances over the years. For these reasons, the PV panel manufacturers are pushing on research and analysis of degradation phenomena, models to reproduce their effect on device performance and testing procedures to determine panel reliability and improve their design. Based on the degradation models, the plant managers can schedule the maintenance and substitution plane for guaranteeing the system performances. The degradation mechanisms involve a gradual reduction of generated power as a function of some environmental parameters, namely temperature, humidity, water infiltration, UV radiation exposure, which determine negative effects due to physical, chemical and mechanisms reactions. The degradation processes differ according to the different materials in terms of quantity and trend over time. The degradation effect can be classified into five types, to which the main performance losses are ascribable:

- *Ageing of semiconductor materials*, ascribable to the introduction of defects into the semiconductor lattice, when PV cells are exposed to harsh operative conditions, such as high temperature and electric field, inducing the migration of atoms and ions. Furthermore, the high relative humidity, UV radiation and thermal cycling can contribute to the active layers' degradation.
- *Degradation of packaging materials*, like protective layer delamination, the breaking of glass, opacification of encapsulation material, and back-sheet infringement reduce harvesting system performances (Fig. 4a, 4b).
- *Loss of adhesion or corrosion of the contacts*, due to the detachment of the Ethylene-vinyl acetate (EVA) protective layer from the back-sheet, not allowing solar radiation to reach the PV panel (Fig. 4c).
- *Failure of cells interconnections*, due to the degradation of solder joints between the cells, caused by the SbPb alloy's segregation, increasing the panel's series resistance and reducing their performance.
- *Deterioration caused by water vapour entry* from the delaminated edges of back-sheet, resulting in contact corrosion and increased current leakages (Fig. 4d).

Also, the migration of metal through the p-n junction as well as the anti-reflective coating corruption represents other performance degradation effects. The effect of dust and dirt on the panel can significantly reduce the solar irradiance and, thus, the conversion efficiency. In [34], authors proposed a model to reproduce dust effect on the conversion efficiency utilizing an experimental setup including two thin-film CdTe solar panels and an MPPT (maximum power point tracker). The experimental results, related to both the clean and dirt panel, agree with those reported in the scientific literature. For detecting the defects above listed, several techniques for fault detection have been developed. In this context, in [35], the authors developed an in-loco inspection system based on photogrammetric thermal analysis with a small drone for determining panel defects, like hot-spots, fault of cell encapsulation and deformation of covering resin. These last induce localized high temperature compared to surrounding area, making them easily identifiable by a thermogram. C. Dunderdale *et al.* proposed a deep-learning and feature-based approach to detect and classify defective PV modules using thermal infrared images [36]. The scale invariant feature transform (SIFT) descriptor, combined with a random forest classifier, allows to identify a working PV panel from a defective one with a significant cost reduction in defects classification. Moreover, the value of series resistance is a good indicator of the health status of the PV panel. In [37], the authors tested two extraction methods (i.e., CGSAA - genetic algorithm and the simulated annealing algorithm and iterative methods) to determine the PV panel's series resistance from I-V characteristics measured under real operating conditions. The extracted parameters were compared with those calculated with empirical laws, obtaining optimal accordance. a-Si PV cells show a power reduction of ~20-30%, after the first exposition to a long-time intense illumination, known as the Staebler-Wronski effect. It is ascribable to the breaking of Si-Si bonds induced by the optically-excited charge carriers, creating defects which in turn cause a reduction of the carriers' lifetime [38].

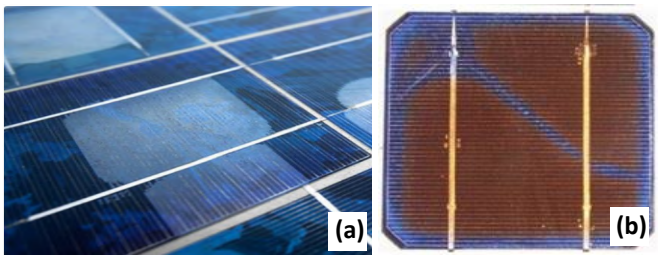

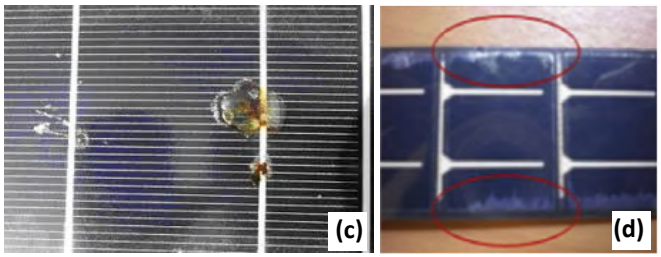

Fig. 4. Examples of typical fails in PV panels: delamination of protective layer (a); encapsulation material browning (b); corrosion of the interconnection line between cells (c); effect of water infiltration from a delaminated edge (d).

Several degradation mechanisms occur in CdTe and CIGS thin-film solar cells, depending on the cell properties and the applied stress. In CdTe PV cells, the copper used to obtain an ohmic contact between the p-type CdTe and the electrodes induce inclusions worsening the cell's electrical performance [39 - 41]. Specifically, the conductivity of the CdTe film is strongly reduced since the copper inclusions introduce recombination centre close to the p-n junction, resulting in a non-ohmic back contact. Also, an applied voltage can deteriorate the CdTe film since it can attract the copper ion near the top electrodes, affecting the cells' open-circuit performances [42]. The introduction of impurities affects the net carrier concentration and open-circuit voltage in CdTe film. In [43], the authors analyzed the effects of impurity diffusion, namely antimony and oxygen, in CdTe films, inferring a correlation between impurities concentration and cell performances. Specifically, for all considered characteristics (V_{OC}, FF, carriers concentration), they reach a maximum value for a given impurities concentration beyond that no further increase has been obtained. Furthermore, Na migration from the front glass into the CdTe film is another deterioration effect in CdTe and CIGS cells. In [44], the authors used transmission electron microscopy to analyze the structural and chemical modification in the CdTe PV panels. They observed an accumulation of Na in the discontinuous part of the CdS layer. Also, they noticed a high accumulation of Na in the TCO/SLG interface, causing the delamination of the conductive oxide from the substrate.

The CIGS PV panels are negatively affected by high temperature and humidity, particularly in flexible solar cells where organic/inorganic coatings are employed [45]. Using x-ray microscopy, in [46], the authors have observed the creation and destruction of defects inside two models of commercial CIGS cells (with large and small grains), acting as recombination centre, thus reducing the diffusion length. The authors observed an increase of voltage ratio, induced by the x-ray beam, with the environmental temperature, in correspondence of defect position, indicating an increase in recombination and bandgap narrowing. Besides, atmospheric gaseous species degrade the performances of CIGS solar cells; in [47], the authors studied the influence of atmospheric gases, such as carbon dioxide (CO_2), nitrogen (N_2), oxygen (O_2) and air on the performances of CIGS PV modules. They demonstrated that the conversion efficiency slightly reduces when the panels are exposed to unpurged water as well as water enriched with O_2 and N_2. This reduction is due to the partial dissolution of ZnO:Al layers, leading to a new intermediate layer, featured by higher series resistance. CIGS panels also suffer from donor-type lattice defects, introducing deep electron traps induced by damp heat treatment, which increases the device's compensation degree and reduces the open-circuit voltage [48].

C. Yang *et al.* studied the effects of strain on the performances of CIGS solar cells [49]. By analyzing the boundary cracks induced by the applied stress, they have derived a multi-linear characteristic between the V_{oc} and I_{sc} parameters, featured by negative coefficients. Furthermore, in [50], the authors developed two experimental setups to carry out combined stress tests in order to evaluate the effects of temperature, humidity, illumination level, and electrical parameters. These setups were used for determining the influence of the deposition conditions and degradation level on the mechanical and electrical stability of CIGS and CZTS solar cells. The Molibdane (Mo) back-contact is a crucial component for solar cell stability since mechanical (due to lack of adhesion) and electrical failures can occur [19].

3.3. Degradation Effects of the III Generation PV Panels

Several protocols have been defined to determine the stability of the organic solar cells, called ISOS tests [51], which ascribe the cells' deterioration to temperature, humidity, oxygen diffusion, UV light, and water infiltrations. These protocols have been employed in several scientific works for determining the OPV lifetime. In [52], the authors have carried out stability tests on ITO-free solar cells over a 2-3 years time period in outdoor conditions; the obtained results demonstrated that oxygen diffusion contributes to cell degradation. Also, K. Kawano *et al.* analyzed the stability of OPV solar cells, realized by a blend of the conjugated copolymers, to different environmental conditions, namely with white light irradiation and in the dark, and under air, dry oxygen and moist nitrogen atmospheres [53]. The experimental results have indicated that the main degradation cause is attributable to the water absorption through the PEDOT: PSS (poly (3,4-ethylene dioxythiophene): poly(4-styrene sulfonate) coating, which induces the increase of the resistance of the interface with the polymer blend. Furthermore, in [54], the authors tested different small-molecules OPV structures under UV illumination in an inert environment. Obtained results indicated a reduction of the V_{oc} up to 25% due to an increase of ITO's work function caused by the reaction with the O_2 plasma. Therefore, a fundamental issue for OPV solar cells concerns the encapsulation; as demonstrated in [55], encapsulated solar cells degrade much less compare to no encapsulated ones, mainly due to the role of oxygen and moisture. Also, exposed OPV exhibited a reduction of I_{sc} within 60% of the initial value, much higher than dark cells, probably due to the increase of trap states or exciton limitation induced by the incident radiation. Moreover, for no encapsulated, the FF quickly reduced due to the air causing some oxidation phenomena. However, the two degradations induce a reduction of the conversion efficiency, mainly ascribable to the I_{sc} reduction. Besides, mechanical stress plays an essential role in the PV cell's stability, mainly for thin-film technologies, since the production process inevitably requires

rolling, bending, and shearing of the polymeric layers. Therefore, optimal resistance and characterization of the polymeric layers to the mechanical solicitations are required [56]. The plastifier addition is a viable way to improve the OPV cells' mechanical stability, reducing the glass transition temperature, young modulus and ductility.

The DSSCs are also subjected to ageing effects due mainly to optical and thermal stress, which modify the cell performances. The main degradation phenomenon in DSSCs concerns the loss of thiocyanate ion ligand of N719 dye, accelerated by the exposition to air and UV radiation, reducing the cell's efficiency. In 2009, Kato *et al.* monitored the behaviour of DSSCs after a durability test last 2.5 years in outdoor conditions [57]. Using the Raman spectroscopy, the authors verified that the TiO_2 electrode impregnated with N719 dye and the counter electrode remained stable. However, the I_{sc} value was unchanged after the durability test, whereas the V_{oc} value and the FF parameter were slightly reduced. These effects were attributable to the increase of the Nerst impedance diffusion triiodide (I_3^-) ions induced by the electrolyte modification over time. L. Ciani *et al.* investigated the ageing effects on DSSCs for different functioning conditions [58]. At first, the DSSCs panels were exposed to prolonged optical stress using a Xe lamp. After several exposition cycles, the authors observed a reduction of the provided current because of a decrease of the redox couples I/I_3 induced by the UV radiation produced by the Xe lamp, thus reducing the ability to produce electrons. Also, the cells were exposed to combined optical and thermal stress at different temperatures. The obtained results demonstrated that exposing the cell at 75°C, a significant reduction of their performance (i.e.V_{oc}, I_{sc}, conversion efficiency) has been observed. This effect is ascribable to significant electrolyte evaporation that occurs at temperatures higher than 75°C, passing through the edge sealing. For unsealed solar cell, a faster reduction of the conversion efficiency was observed in [59]. Furthermore, beneficial effects have been demonstrated by adding MWCNTs to the TiO_2, reducing the drop in efficiency compared to the cells based on pure TiO_2 [60]. The authors have supposed that the addition of the MWCNTs network inside the anode limits the recombination of the photo-induced charges.

The perovskite solar cells are affected by a stability issue, limiting their applicability in a real-life scenario. Several scientific works have shown that perovskite material ($CH_3NH_3PbI_3$), the most used active material, is intrinsically unstable because of its hygroscopicity, and UV sensitivity, inducing its parasitic conversion in PbI_2 and CH_3NH_3I. In particular, in [61], the authors employed the laser beam induced current (LBIC) method to determine the degradation of PSCs caused by moisture. The authors have identified different deterioration mechanisms ascribable to both perovskite material and the hole transport material (HTM), and so they suggested a strategy for increasing the stability of the perovskite solar cells. Besides, ion migration represents a problem for PSCs, since mobile ions degrade perovskite over time; they cause a current/voltage hysteresis, modifying the active material's bandgap locally, reacting with the ETM and HTM, and leading to several issues [62]. Also, the oxygen diffusion inside the perovskite can negatively influence the solar cell's performance and stability [63]. The scientific community has widely analyzed the effect of UV light-induced degradation of the perovskite material. The UV-radiation induces competing generation and destruction of defects acting as carrier traps, thus reducing the cell efficiency [64]. Moreover, M. Saliba *et al.* have analyzed the ageing behaviour and stability of PSCs [65]; they demonstrated that the PSCs shows a very unusual behaviour compared to other cell typology since feature by time-dependent ageing. PSCs present a hysteresis of I-V characteristic during the MPPT, reversible placing the cell in the dark. This effect must be considered when the PSCs work in a real scenario, hence subjected to day/night alternation.

4. Methods for Predicting the Solar Energy of the PV Panels

Energy prediction is a topic of high interest. In Fig. 5, a taxonomy of the different methods employed to predict the PV produced energy is shown. In particular, our analysis has focused on matrix and mother-PV methods in a detailed manner. The first one is a simple solution for predicting the produced energy by solar cells on the basis of direct measurements carried out in real working conditions [66, 67]. The PV energy that could be provided by a PV module, over a period of one year, is obtained by multiplying the power matrix elements, $\boldsymbol{P}=\{P(Gi, Ta)\}$ with those of the climatic events matrix $\boldsymbol{N}=\{N(Gi, Ta)\}$ and then adding the terms of the matrix obtained in this way:

$$E = \sum_{Gi,Ta} P(Gi,Ta)N(Gi,Ta)[kWh/year] \quad (10)$$

The power matrix $\boldsymbol{P}=\{P(Gi, Ta)\}$ has information on the produced PV power depending on the incident radiation (G_i) and room temperature (T_a). The **P** matrix elements $P(Gi, Ta)$ are obtained using the average of the power values provided by the panel under measurement for one year, for each different climatic situation (G_i, T_a):

$$P(Gi,Ta) = \frac{1}{N}\left(\sum_{i=1,\ldots,N} P_i(G_i,T_a)\right) \quad (11)$$

name of method	from	power or efficiency equations	temperature coefficient(s)
SSE	CREST	$\eta(G,25°) = C_0+C_1G+C_2\ln G$	TC@1000W/m²
Yield Simulator	ECN	avg $\eta(G,25°)$	average TC (250,500,750,1000W/m²)
Somes	UU	$P_i = P_{nom}\frac{\Theta(G)}{\Theta(1000)}\frac{G}{1000}$	TC=0.4%/°C (default value)
MotherPV	INES	avg $\eta(G,25°)$	TC(G)
PV-SAT	H2M	$\eta_{MPP}(G,T) = a_1 + a_2G + a_3\ln(G\cdot m^2\cdot W)\cdot(1+\alpha\cdot(T-25))$	
Matrix method	SUPSI	$I_m = I_{m,STC}\,G/1000\,[1+\alpha_{Im}(\Delta T + T - 25)]$ $V_m = V_{m,STC}+C_0\ln(G/1000)+C_1(\ln(G/1000))^2+\beta_{Vm}(\Delta T+T-25)$	
ESTI-ER	JRC	$P(G,T)= I_{m,STC}\,G/1000\,[1+\alpha_{Im}(T-25)](V_{m,STC}+C_0\ln(G/1000)+C_1(\ln(G/1000))^2+\beta_{Vm}(T-25))$	
ZENIT	ISE	$P(G,T) = a\cdot G^2 + b\cdot\log(G+1)\cdot G + c\cdot\left(\frac{(\log(G+e)^2)}{G+1}-1\right)\cdot G + d\cdot(T-25)$	

Fig. 5. Taxonomy related to PV energy prediction methods.

Each P(Gi, Ta) matrix element is obtained by multiplying I_m and V_m values related to specific solar radiation and climatic conditions (G_i, T_a). Lastly, the obtained matrix is "filtered" by eliminating those points with a frequency of less

than 3 (N<3, i.e. rare events) or resulting from measures with high standard error (S_tD_{ev}/A_{vg} > 20%, i.e. a wrong measure). The climatic events matrix $N(G_i, T_a)$ counts the number of times that a determinate climatic event (G_i, T_a) occurs in a year, information that can be obtained by the hourly data of radiation and temperature by employing a standard online weather software (e.g. Meteonorm), or by means of the direct acquisition of (G_i, T_a) values using a climatic station located near the PV panels. In the latter case, the obtained matrix values have to be normalized by dividing them for the acquisitions' number in an hour. The procedure to obtain the P(Gi, Ta) matrix consists of a separated interpolation of the current $I_m(Gi,T_a)$ and voltage $V_m(Gi,T_a)$ values acquired by the carried out measures. Then, the power matrix is obtained by multiplying the matrix of current values with that related to the voltage ones. The used equations are reported below:

$$I_m = I_{m\,stc} \cdot \frac{G_i}{G_{i,stc}} \cdot [1 + \alpha_m \cdot \left(\Delta T \cdot \frac{G_i}{G_{i,stc}} + T_a - T_{a,stc}\right)] \quad (12)$$

$$V_m = V_{m,stc} + C_0 \cdot \ln\left(\frac{G_i}{G_{i,stc}}\right) + C_1 \cdot \ln\left(\frac{G_i}{G_{i,stc}}\right)^2 + \beta_{Vm} \cdot \left(\Delta T \cdot \frac{G_i}{G_{i,stc}} + T_a - T_{a,stc}\right) \quad (13)$$

Being $I_{m,stc}$ the current at maximum power point (MPP) in Standard Test Conditions (STC), α_{Im} the temperature coefficient of I_m and $\Delta T = (T_{cell}-T_a)$ both for a solar irradiance value of 1000 W/m^2, $V_{m,stc}$ the voltage at the MPP in STC, C_0 and C_1 parameters of the PV panel, β_{Vm} the temperature coefficient of V_m, T_a the room temperature, and G_i the incident radiation on the PV panel [68, 69].

Instead, the MotherPV method employs the normalized distribution function (DF) of the solar resource (SR), expressed in Sun's hours as a function of the solar irradiance expressed in Suns, with steps of 0.025 Suns. Using this discretization, the SR is fully represented by an easily readable table consisting of approximately 50 lines. According to the scientific literature, the DF must not be calculated with time intervals between the irradiance measurement instants larger than 5 min. In particular, time intervals extended up to one hour lead to large not-acceptable errors in the real DF of SR [70]; this is easily understandable since during windy days but with the presence of the sun and isolated clouds, the average value of solar irradiation in one hour suppresses the high variations (low and high values) of irradiation from the statistics. In [71], the authors proposed a new model, applicable to the MotherPV method, for reproducing the irradiance coefficient as a function of the irradiance level, for six PV technologies, including the thin-film ones (CdTe and CIS). This model was compared with other ones reported already in the literature. The proposed model provides the best accuracy compared to the other ones, especially for thin-film technologies.

A short-term energy prediction method, as a function of panels ageing, is the topic of this work. PV panel ageing alters its performances and makes the utilization puzzling in a context of an extended wide grid. Testing ageing phenomena requires compulsory and precise calibration of the characterization architecture, especially instruments and panels [72]. Ageing is mostly due to two main causes, intrinsic and environmental ones [34,73]. The first is due to defects related to the fabrication process and environmental reasons, bringing to heavy dust able to attack the panel materials, and to high operating temperature. Figs. 6 and 7 depict intrinsic defects and attacking dust inside and on the panel that greatly reduce its performance; in particular, Fig. 6 is taken from a real case studied in our laboratory, where the testing architecture, described in the next section, is located; it also illustrates three critical points on the surface due to probable bad deposition of Si-monocrystalline.

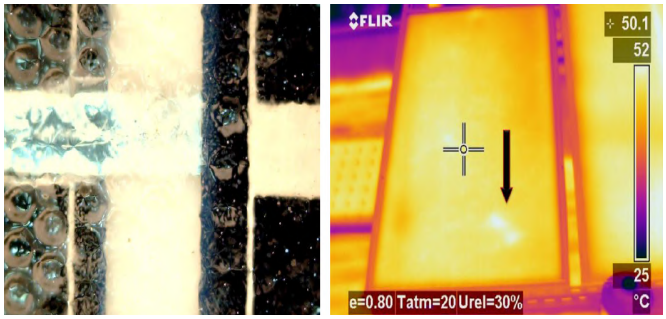

Fig. 6. Intrinsic defects: zoomed digital imaging (left) and corresponding thermal imaging (right).

Fig. 7. Dust deposition on the PV panels.

5. Experimental architecture for MPPT devices calibration

Two identical PV panels were used (i.e. TPS-105 175 W Si-monocrystalline model) for the MPPT calibration. The developed measurement apparatus is shown in Fig. 8; the most important element in the acquisition system is the Maximum Power Point Tracker (MPPT), an electronic device that acts on the PV modules varying continuously their operating point, to provide the MP they are capable of [74,75]. As depicted in Fig. 8 and 9, the used MPPT is an electronic system, not a mechanical one, able to continuously move the PV panels to follow the daily movement of the sun and so maximize energy production [76,77]. Its technical features parameters are following reported:

- High accuracy of the MPP tracking, P_{max} (W) [74];
- Simultaneous I_m and V_m measurement with wide voltage and current ranges (up to 200V / 20A / max 250W);
- Temperature detection by 4 PT100 sensors located under each PV module and connected to the data-logger;
- Irradiance in W/m^2 using a CM11 pyranometer;
- Galvanically isolated RS-485 interface: a dialogue between the PC master and one or more MPPTs;

- I-V Tracer: use of the MPPT3000 as settable IV Tracer;
- Environmental parameters, namely air temperature, humidity level, wind intensity and direction, by means of auxiliary sensors.

The data acquisition system, included in the measurement chain, acquires the voltage and current values provided by PV modules, their temperature through the Agilent 34970 data-logger, and environmental parameters including the air temperature, solar irradiance level and wind intensity by using a WS3650 wireless weather station (as shown in Fig. 8). The block scheme of the multi-parameter data acquisition electronic apparatus, shown in Fig. 8, has the MPPT 3000 in the center, with indicated its connections with all other sections [67, 78]. The employed MPPT is made up of three modules connected to each other: the control board, the power board and one for the user interface (Fig. 9); it allows users to trace the I-V curve of the under-test PV panels and to acquire up to three signals coming from connected transducers. For interacting with the MPPT, it is possible to use some buttons and LCD or through the graphic interface of the software installed on the PC. The produced power is dissipated by a resistive load connected to the MPPT output. After the description of the experimental measurement and characterization chain, the calibration scheme is shown in the following Fig. 10 and Fig. 11. The reason of the experimental setup shown in Fig. 10 and 11 is double: (a) both MPPTs, due to previous technical failures, have to be re-calibrated before using them in the testing system beside the others; (b) the calibration operation must be performed, in real conditions, in a short time by addressing technical requirements for long term testing.

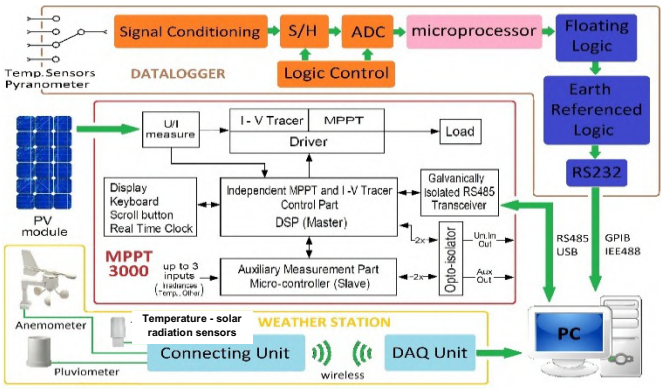

Fig. 8. Block scheme of data acquisition apparatus to detect interest parameters and optimize PV panels' working point.

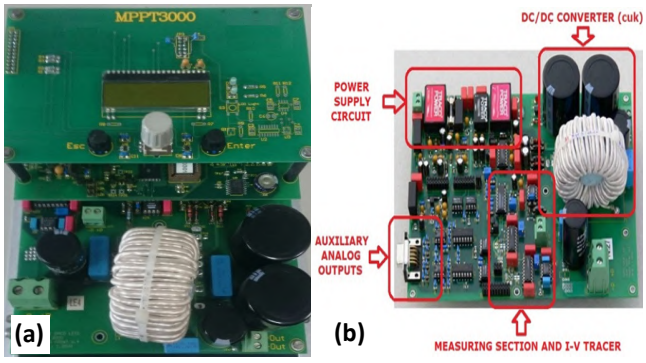

Fig. 9. Internal photo of the used MPPT3000 device (a); MPPT power board with highlighted the different sections.

So, we used a *Microcal 20* calibrator [79] inserted in the envisaged chain, using also resistors connected in voltage and current divider configurations; thereby, the acquired voltage and current values cannot overcome the maximum values for the calibrator (i.e 20 V and 50 mA respectively). Fig. 10 illustrates the adopted experimental measurement setup for the calibration of two MPPTs simultaneously, in particular for detecting the PV module's current (on the left) and the voltage (on the right) [80].

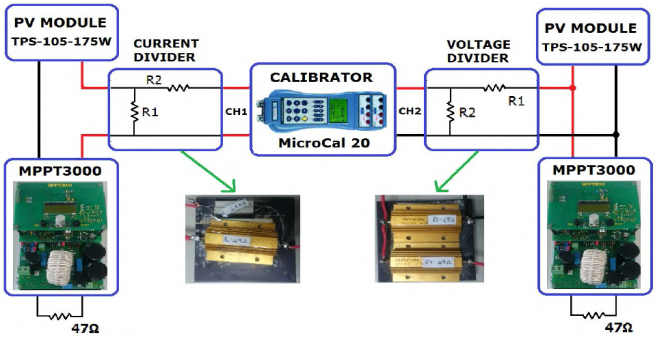

Fig. 10. Detailed scheme of the calibration architecture.

Fig. 11. Electric connections with *MicroCal 20* calibrator.

The calibrator, used as a reference measuring instrument, measures at the same time, as well as also the MPPTs, the voltage and current values generated by two PV modules using its two channels. As the MPPT, the MicroCal 20 calibrator has embedded data logger function to save the detected data in its embedded memory device with *.csv* format, to be, after downloaded by RS232 serial port. Current and voltage values provided by both PV panels are stored and displayed through a dedicated software, as depicted in Fig. 12, together with the IV characteristic curve of under-test PV panel.

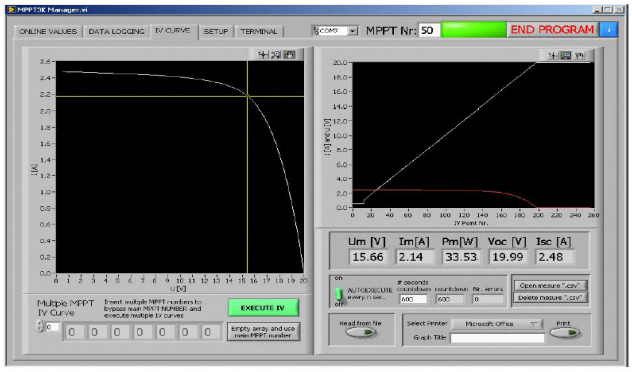

Fig. 12. I-V curve of the under-test PV panel displayed by MPPT software.

6. Experimental results and Related Discussion

Based on previous architecture and setup, we performed tests on several days in December, on the roof of Dept. of Innovation Engineering-Salento University, where the lab is located (GPS coordinates: 40.335273, 18.114991). The main scopes of the experimental activity are the calibration of the two MPPTs [81], repaired during the maintenance process, and performing a power prediction in a short time, which is very difficult. The experimental setup, reported in Fig. 13, includes two Si-monocrystalline panels (TPS-105 175 W) used for the MPPTs calibration, as well as four CdTe and one CIGS PV modules (shown in Fig. 13a and 13b, respectively) for performing electrical measures to predict, then, the produced energy in a year. Fig. 13b shows the CIGS module and the Klipp-Man CM11 pyranometer used to perform the panel's characterization (Fig. 13c and 13d). The CM11 pyranometer measures the irradiance (W/m^2), resulting from solar radiation and passing through the protective hemispherical cover. It is featured by a wide detection range (310÷2800 nm), a sensitivity from 4 to 6 $\mu V/m^2$, and temperature dependence lower than 1%.

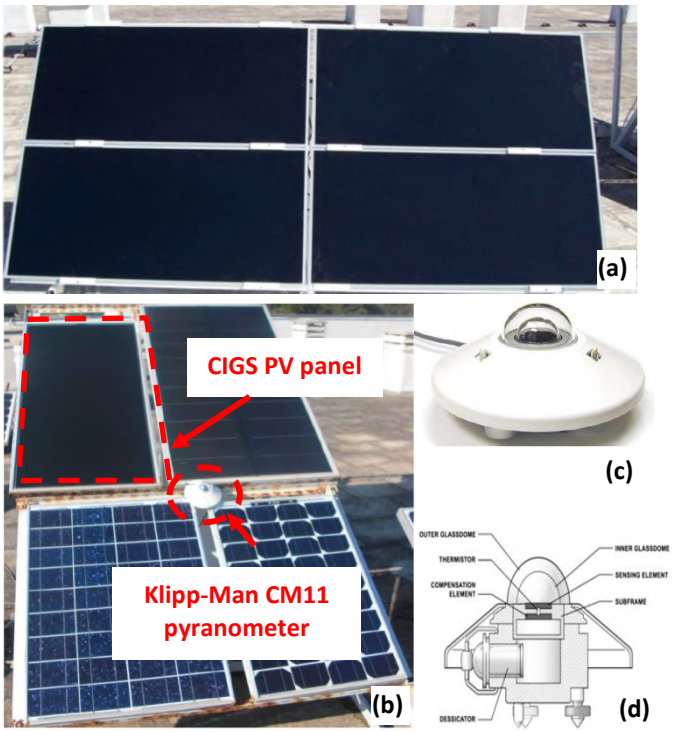

Fig. 13. CdTe modules located on the rooftop of Dept. of Innovation Engineering (Univ. of Salento) (a). CIGS panel mounted on support structure with CM11 pyranometer (b). Detail of Klipp-Man CM11 pyranometer (c) and schematic representation with highlighted the main components (d).

The tested CdTe panels are FS-275 model, manufactured by *First Solar Co.*, whereas CIGS PV module is produced by Eterbright *s.r.l.* (model CdF-1000A1). The main features of the employed PV panels are summarized in Fig. 14. The first series of calibration yields to Fig. 15, showing plots, as a function of time, related to the voltage values provided by Si-monocrystalline PV panels, measured simultaneously by both the Micro-Cal calibrator (V_{CAL}) and MPPT (V_{MPPT}) for verifying the proper calibration of the MPPT device; β_V is the multiplication coefficient due to resistive divider. Comparing the two plots, the difference between V_{MPPT} and V_{CAL} x β_V represents the MPPT voltage error (ΔV). In Fig. 16, the current values detected at the same time through the MicroCal calibrator and MPPT are plotted, to certify the MPPT calibration after technical intervention for repair; differences between I_{MPPT} and I_{CAL} x β_I represent MPPT error (ΔI) in the current measurement. All plots have time as the horizontal axis, with an observation period between 12 up to 4 pm. It is crucial to notice that used resistances are Arcol HS100-47J with the following values: for voltage-divider $R_1=R_2=47\Omega$, for the current-divider R_1= 4.1 Ω and R_2=47 Ω.

Parameter	*First Solar*-275	*Eterbright CdF-1000A1*
Nominal Power [W]	75	110
Power tolerance	±5 %	±5 %
V_{oc} [V]	92	73.4
I_{sc} [A]	1.2	2.1
V_{MPPT} [V]	69.4	56.9
I_{MPPT} [A]	1.2	1.93
Maximm Volt. [V]	1000	1000
Size	600 mm x 1200 mm x 68 mm	652 mm x 1234 mm x 35 mm

Fig. 14. Table with the specifications of tested PV panels.

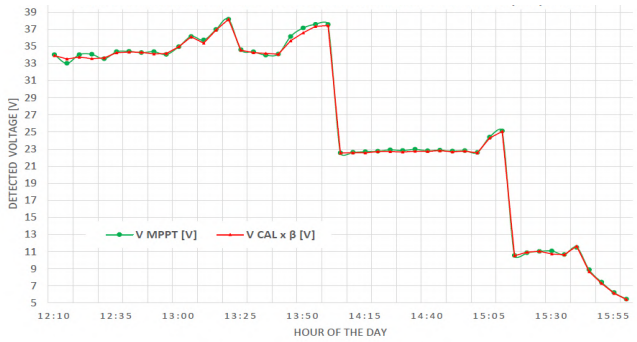

Fig. 15. Plots as function of time of voltage values acquired by the Micro-Cal calibrator and MPPT simultaneously to certify the MPPT's calibration.

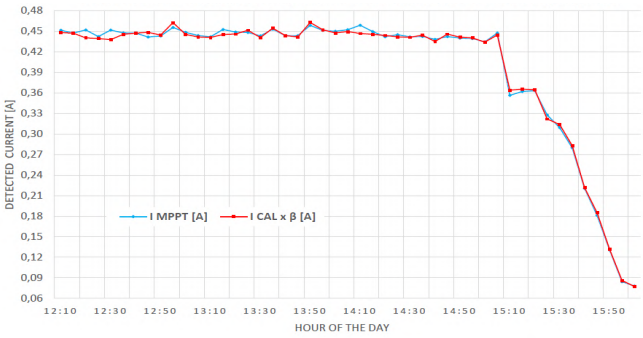

Fig. 16. Graphs with respect to time relative to the current values detected by Micro-Cal calibrator and MPPT simultaneously to certify the proper MPPT calibration.

Continuing on the same reflection, below other voltage and current plots are shown (Fig.. 17 - 18 and Fig. 19 - 20, respectively), related to the following winter days; all temporal trends are correctly justified and agree with weather conditions of those days, available through the wireless weather station on-site (Fig. 8) [82].

Fig. 17. Graphs with respect to time relative to voltage values by calibrator and MPPT; rapid variations (orange boxes) due to MPPT operating point changes to maximize the extracted PV power following a solar radiation reduction.

As we obtained a database of all parameters, we compared these data (related to only 5-7 days), with those available for the same days in the five-ten previous years (i.e. from 2014 to 2018). Obviously, the interesting parameter is the solar radiation for these five years [83 - 85].

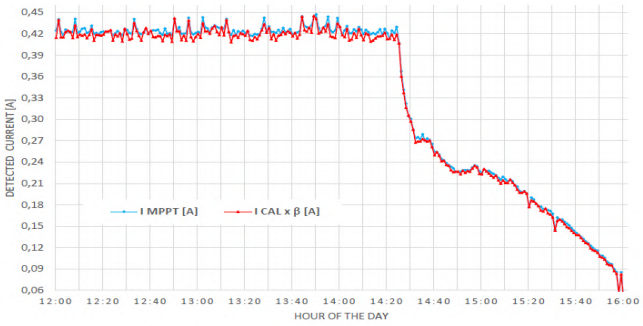

Fig. 18. Graphs with respect to time relative to current values obtained by the MicroCal 20 calibrator and MPPT and related to Fig. 17 voltage plots.

Fig. 19. Graphs with respect to time relative to detected voltage values by means of the calibrator and MPPT; the negative peak, in the blue box, due to solar radiation's reduction for some clouds covering the sun.

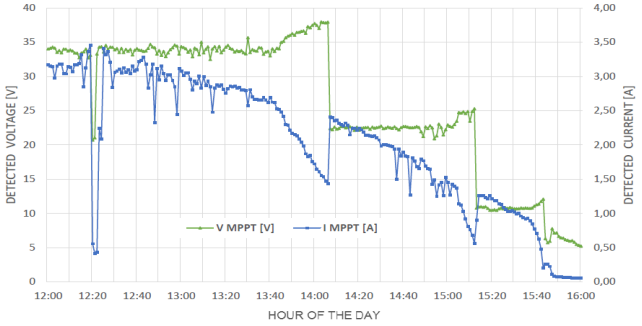

Fig. 20. Time trends of current/voltage detected by MPPT.

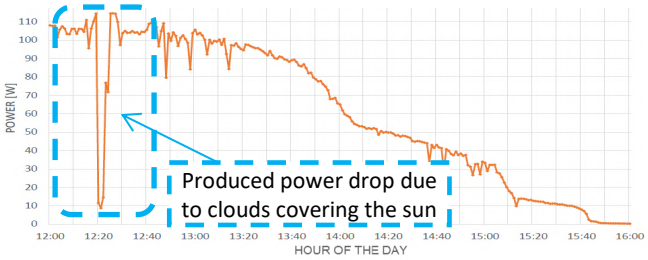

Fig. 21. Extracted power from the under-test PV panel, referring to current and voltage values shown in Fig. 20 and detected by the calibrated MPPT 3000.

Then, Figures 22 (a, b, c) illustrate 3-days cumulative radiation trends; it means that we summed all solar radiations for same days and acquisition steps for five different years, to be able to understand in depth the PV panels behaviour and performance as well as to have a good database for comparisons and metrics [15 - 17].

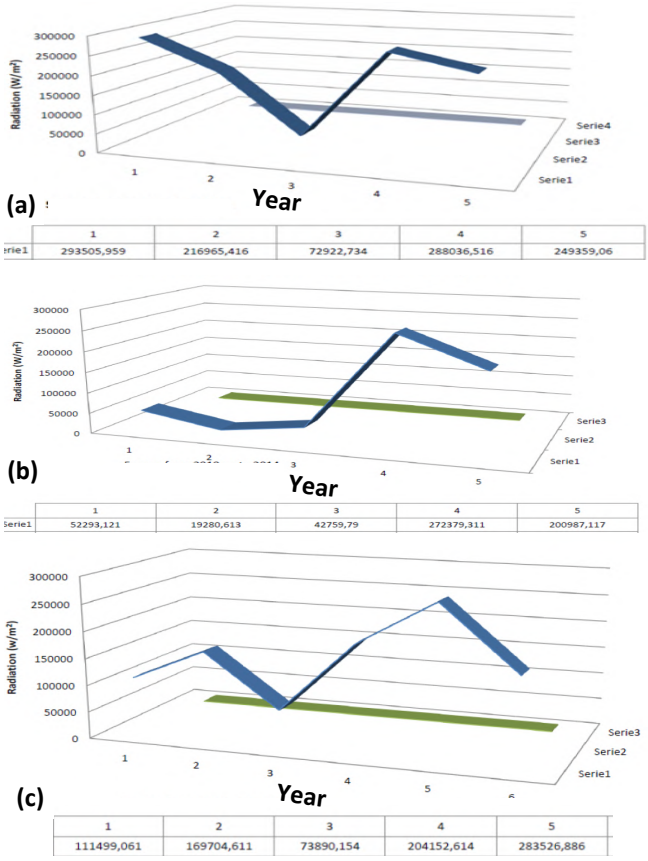

Fig. 22. Total solar radiation for 3 december days in 5 years.

After the MPPTs calibration, the power measurements for both CdTe and CIGS PV panels have been performed and compared with the data predicted by using the matrix method. Below, only the data related to the CIGS panel has been reported for three different days. The I-V characteristic determination is based on current and voltage measurement through resistances at the terminal ends of PV panel. Hence, in ideal conditions, the power dissipated through resistances has to be equal to the maximum power retrieved through MPPT. So, we proceeded with the calculation of the equivalent power dissipated through resistances, given by:

$$P_{eq} = R_{eq} \cdot I_{MPPT}^2 \quad (14)$$

where R_{eq} varies according to the used configuration, that is voltage or current divider. The measurements are affected by some uncertainty, mainly due to resistances since the MPPT uncertainty is neglected [86]. The uncertainty of type A, thanks to datasheets, is computed according to:

$$U_T = \sum_{i=1}^{N} \frac{\partial f}{\partial y_i} U_i \qquad (15)$$

Eq. (15) allows us to determine the uncertainty affecting R_{eq}; f represents the functional relationship of used divider, y_i stands for each involved parameter. The PV produced power, just for 3 days, is displayed in Fig. 23 (a, c, and e), calculated as $P_{MPPT} = V_{MPPT}\ I_{MPPT}$, P_{eq} and $P_{Umax} = (R_{eq} + U) \cdot I^2_{MPPT}$. According to datasheet, uncertainty of voltage and current dividers are 10% and 5%, respectively, according to the resistance features. The issue of produced power is crucial since our aim is to predict, by a short-time analysis, energy production throughout the year, by means of the power measurements carried out in outdoor tests, over a narrow observation time. In Fig. 23 (b, d, and f), the power estimated by the matrix method as a function of the solar radiation G (W/m^2), obtained by CM11 pyranometer, is shown relative to power graphs of Fig. 23 (a, c, e) [87]. By observing power trends over-time in Fig. 23 (a, c, e), we certified the correct calibration of repaired MPPTs obtained by the MicroCal 20 calibrator-based measures previously shown in Figures from 15 to 19 [88]. Also, by comparing them with the respective Figs. 23 (b, d, f) obtained by the matrix method to predict the energy production, an excellent agreement has been found, taking into account the uncertainty and data processing [89].

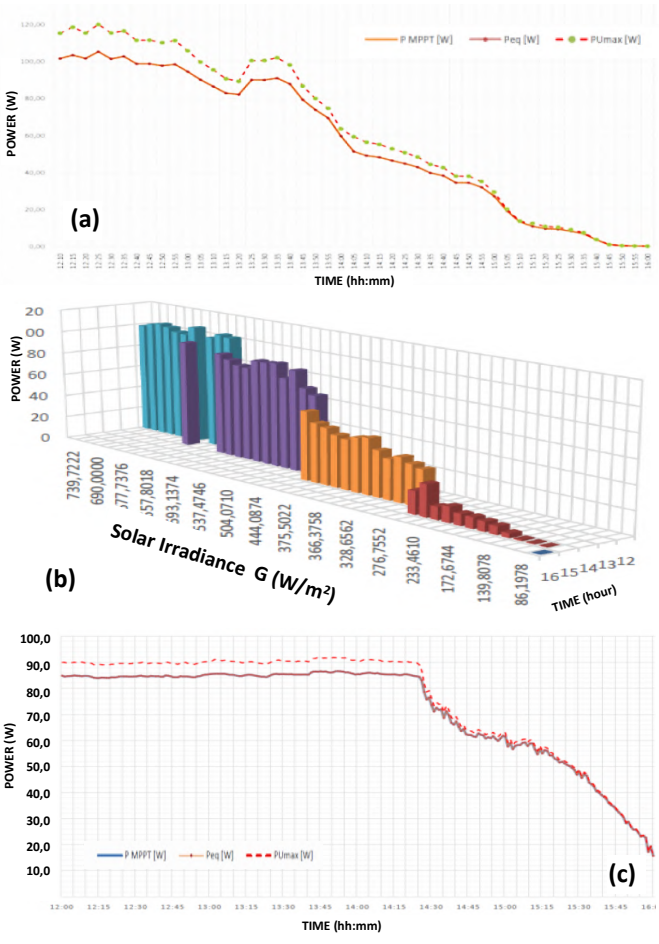

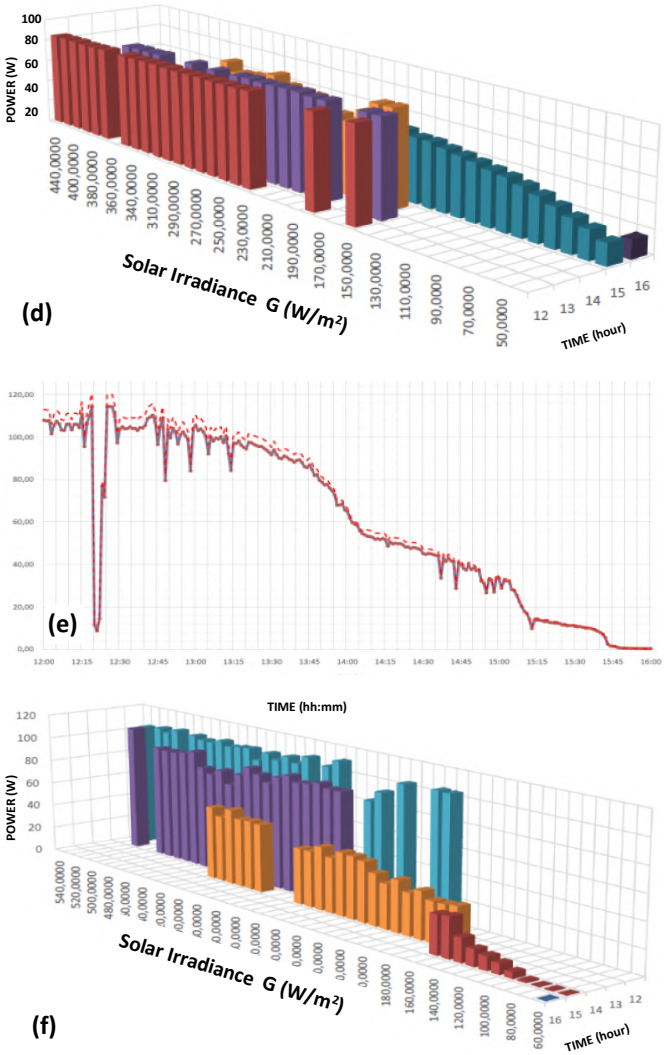

Fig. 23. Graphs as a function of time of power produced by the under-test CGIS panel (Eterbright CdF-1000A1) for 3 different days (a, c, and e), calculated as P_{MPPT}, P_{eq} and P_{Umax}; histograms related to estimated power by the matrix method, as a function of solar radiation values, for same days (b, d, f).

The power matrix, described in Eq. (11) and determined by temperature (T_a) and solar incident radiation values (G_i) (i.e. the climatic condition matrix $N(G_i, T_a)$, Eq. (10)) thanks to the used weather station (Fig. 8), allows us to correctly predict PV energy production and to better understand the capability of each solar panel or plant to generate the required energy, not being able to rely only on technical features and performance declared at STC by the manufacturer. In this regard, energy prediction methods are crucial as they can also take into account, statistically, the ageing factors that degrade the panels' efficiency, over time, often in a random manner. With a minimum database (panels type, electrical parameters, orientation and inclination of PV system, installation site and weather data easily available, e.g through the Meteonorm website), the energy production can be estimated with a good level of precision.

The degradation of PV modules is commonly expressed in terms of degradation rate (R_d), representing the parameter (Y) reduction from the initial value (Y_0) (defined as G_d-global degradation) over a given observation interval (Δt):

$$R_d(Y) = \frac{G_d(Y)}{\Delta t}\left[\frac{\%}{year}\right] \quad (16)$$

$$G_d(Y) = \left(1 - \frac{Y}{Y_0}\right) * 100\ [\%] \quad (17)$$

The parameters usually considered for the calculation of G_d are the maximum power (P_{max}), maximum current (I_m), maximum voltage (V_m) and FF. In [90], the authors monitored the degradation rates of different PV modules, both in Si-monocrystalline and thin-film technologies and in several operative conditions. The results demonstrated that the average R_d values were equal to 1.50 %/year and 1.73 %/year for Si-monocrystalline and thin-film technology panels, respectively. Furthermore, M. Demirtas *et al.* evaluated CdTe and CIS PV modules' performances over 3-5 years, collecting their electrical parameters [91]. The final results indicated that 14.49% and 21.24% power losses were obtained for CdTe and CIS PV panels, also due to the presence of micro-cracks and delamination. In [92], the authors analyzed the performance loss rates and seasonality of 11 PV plants based on different technologies, including CdTe and CIGS ones. The plant performances were expressed in terms of R_p defined as the ratio between the actual energy production at the end of the year and the nominal plant output. Using CSD (classical seasonal decomposition) on five years measurements, the results indicated that the performance loss rate for CIGS technology was 2.35 %/year (using First Solar FS60 model), whereas 2.42 %/year for the CdTe technology (using Würth Solar 11007/75 model) (Fig. 24). Also, we monitored the annual energy production for our thin-film PV panels over a 10 year observation period. In particular, a performance loss of 3.23 %/year has been observed for the CdTe PV panels, as well as a 2.76 %/year for CIGS ones. The obtained results agree with those reported in literature [92], with a difference of +0.81% and +0.41%, for CdTe and CIGS PV panels, respectively.

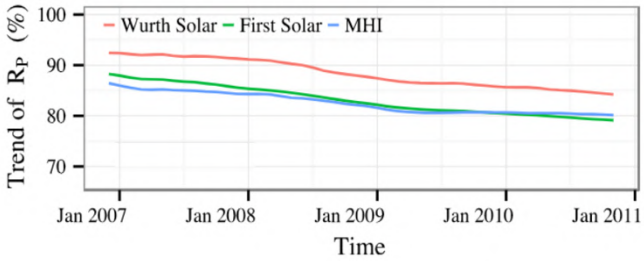

Fig. 24. Performance ratio trends over five years for different technologies (i.e. CdTe (red), CIGS (green) and a-Si (blue)).

7. Conclusions

The ageing effects of PV panels are extensively analyzed by the companies and scientific community to develop predicting methods of their provided power over time. This research provides, at first, a comprehensive overview of the ageing mechanisms in II and III generation PV panels and the most used predicting methods. Afterwards, an experimental measuring apparatus was presented for proper calibration and operating mode check of MPPT devices, that need to be calibrated after any repairs, directly connected to the PV panels; a low measurement error (< 1,5%) was determined by comparing the current and voltage values measured by MPPT with those supplied by a reference measuring instrument. Besides, we demonstrated that short term-based measurements of the produced power from under-test panels can be properly used to estimate energy, by using the matrix method, over a wider period on the proviso that a correct database related to long term-based measurements are available for a comparison. The realized site with PV panels' installation has a database over 10 years long related to the produced power, as function also of the solar irradiance and temperature values for different panels technologies [66, 67]. Presented experimental approach is not always easy and reliable in those regions with four seasons and frequently changing weather conditions, but the use of calibrated MPPT in appropriate measurement system with available long-term measures database, makes it easier.

Nomenclature

PV	Photovoltaic panel	I_{MPPT}	Current value measured by the MPPT [A]
CIGS	Copper Indium Gallium diselenide	I_{CAL}	Current value by the Micro-Cal calibrator [A]
CdTe	Cadmium telluride	I_0	Dark saturation current [A]
a-Si:H	Hydrogenated amorphous silicon	I_{ph}	Photo-generated current [A] (Eq. 1)
CIGS	Indium copper gallium diselenide	$I_{m,STC}$	Current at the MPP in STC [A] (Eq. 12)
GaAs	Gallium arsenide	P_{max}	Maximum power [W]
OPV	Organic Photovoltaics	P_{th}	Theoretical power provided by PV panel [W]
DSSCs	Dye-Sensitized Solar Cells	P_{eq}	Equivalent power dissipated through resistances
CZTS	Zinc Tin Sulphide	P_{MPPT}	Power measured by the MPPT
PSC	Perovskite solar cells	P_{Umax}	Maximum power dissipated by the R_{eq} resistance
ITO	Indium Tin Oxide	P_{input}	Incident luminous power [W] (Eq. 7)
EVA	Ethylene-vinyl acetate	P_{output}	output electrical power [W] (Eq. 7)
MPPT	Maximum Power Point tracker	***P***	Power matrix
LBIC	Laser beam induced current	P(Gi, Ta)	Element of power matrix
HTM	Hole transport material	**N**	Climatic Event Matrix

ETM	Electron transport material	N(Gi, Ta)	Elements of the matrix of the climatic events
V_{oc}	Open-circuit voltage [V]	k_B	Boltzmann Constant
V_m	Maximum voltage[V]	q	Electron charge [C]
V_{MPPT}	Voltage value measured by MPPT	R_{eq}	Equivalent resistance of voltage/current divider
V_{CAL}	Voltage by Micro-Cal calibrator	STC	Standard test conditions (T = 25 °C, G= 1000 W/m^2 and AM = 1.5)
$V_{m,STC}$	Voltage at MPP in STC [V] (Eq. 13)	E_g	Energy gap (eV) (Eq. 2)
I_{sc}	Short circuit current [A]	UV	Ultra-violet
I_m	Maximum current [A]	FF_0	Ideal fill factor
DF	Distribution function	FF	Real fill factor
SR	Solar resource	Φ	Photon flux
ΔV	Voltage error [V]	Gi	Incident radiation
ΔI	Current error [A]	G	Solar irradiation on a model plane [W/m^2]
η	Conversion efficiency	f	Functional relationship of used divider (Eq. 15)
η_{max}	Maximum conversion efficiency	y_i	Parameter involved in the voltage divider relationship (Eq. 15)
A	Panel Area[m^2]	U_i	Uncertainty affecting R_{eq} related to y_i parameter
T_a	Ambient temperature [K]	U_T	Total uncertainty affecting R_{eq}
T_c	Cell temperature Tc [°C]	S_tD_{ev}	Standard deviation
ΔT	Temperature difference between air and cell [°C]	A_{vg}	Average
f_0	Corrective factor for panel area (Eq. 2)	α_{Im}	Coefficient of temperature of I_m [°C^{-1}] (Eq. 12)
E	Energy produced in a year [Wh/year]	C_0	Parameters of the PV panel (Eq. 13)
$G_{i,stc}$	Solar irradiance defined by the STC conditions (1000 W/m^2)	C_1	Parameters of the PV panel (Eq. 13)
$T_{a,stc}$	Ambient temp. STC conditions (25 °C)	β_V	Multiplication coefficient due to voltage divider
RMSE	Root Mean Square Error	β_{Vm}	Temperature coefficient of V_m [°C^{-1}] (Eq. 13)
LID	Light-induced degradation	IR	Infrared
R_p	Performance ratio	R_d	Degradation rate

References

[1] K. Nishioka, T. Takamoto, T. Agui, M. Kaneiwa, Y. Uraoka, T. Fuyuki, "Evaluation of InGaP/InGaAs/Ge triple-junction solar cell and optimization of solar cell's structure focusing on series resistance for high-efficiency concentrator photovoltaic systems," *Solar Energy Materials and Solar Cells*, vol. 90, pp. 1308–1321, May 2006, DOI: 10.1016/j.solmat.2005.08.003.

[2] K. Neuhaus, C. Alonso, L. Gladysz, A. Delamarre, K. Watanabe, and M. Sugiyama, "Solar to Hydrogen Conversion using Concentrated Multi-junction Photovoltaics and Distributed Micro-Converter Architecture," *7th IEEE Int. Conf. on Ren. Energy Res. and Appl.*, Paris, October 2018, 744–747.

[3] A. H. Dida and M. Bekhti, "Study, modeling and simulation of the electrical characteristic of space satellite solar cells," *6th IEEE Int. Conf. on Ren. Energy Res. and Appl.*, San Diego, November 2017, 983–987.

[4] Berardone, M. Paggi, "Nondestructive monitoring of damage caused by accelerated ageing in photovoltaic modules," *Proc.of the Inst. of Mechanical Engineers, Part C: J. of Mechanical Engineering Science*, vol. 233, pp. 1-19, Dec. 2019, doi: 10.1177/0954406219889382.

[5] G. C. Eder, Y. Voronko, S. Dimitriadis, K. Knöbl, G. Újvári, K. A. Berger, M. Halwachs, L. Neumaier, C. Hirschl, "Climate specific accelerated ageing tests and evaluation of ageing induced electrical, physical, and chemical changes," *Progress in Photovoltaics: Research and Applications*, vol. 27, no. 11, pp. 934–949, 2019, DOI: 10.1002/pip.3090.

[6] M. Boussaid, A. Belghachi, K. Agroui, N. Djarfour, "Mathematical models of photovoltaic modules degradation in desert environment," *AIMS Energy*, vol. 7, no. 2, pp. 127–140, 2019, DOI: 10.3934/energy.2019.2.127.

[7] B. Nehme, N. K. M'Sirdi, T. Akiki, and A. Naamane, "Contribution to the Modeling of Ageing Effects in PV Cells and Modules," *Energy Procedia*, vol. 62, pp. 565–575, Jan. 2014, DOI: 10.1016/j.egypro.2014.12.418.

[8] J. D. Bastidas-Rodríguez, E. Franco, G. Petrone, C. A. Ramos-Paja, G. Spagnuolo, "Model-Based Degradation Analysis of Photovoltaic Modules Through Series Resistance Estimation," *IEEE Trans. on Industrial Electr.*, vol. 62, no. 11, pp. 7256–7265, Nov. 2015, DOI: 10.1109/TIE.2015.2459380.

[9] S. Lindig, I. Kaaya, K.A. Weiss, D. Moser, and M. Topic, "Review of Statistical and Analytical

Degradation Models for Photovoltaic Modules and Systems as Well as Related Improvements," *IEEE Journal of Photovoltaics*, vol. 8, no. 6, pp. 1773–1786, Nov. 2018, DOI: 10.1109/JPHOTOV.2018.2870532.

[10] H. Maammeur, A.Hamidat, L. Loukarfi, "A numerical resolution of the current-voltage equation for a real photovoltaic cell", *Energy Procedia*, vol. 36, pp. 1212 – 1221, December 2013.

[11] P.Visconti, P. Costantini, C. Orlando, G. Cavalera, A. Lay-Ekuakille, "Software solution implemented on hardware system to manage and drive multiple bi-axial solar trackers by PC in photovoltaic solar plants", *Measurement*, vol. 76, pp. 80 – 92, December 2015.

[12] L. X. Wang, Z. Q. Zhou, T. N. Zhang, X. Chen, M. Lu, "High fill factors of Si solar cells achieved by using an inverse connection between MOS and PN Junctions", *Nanoscale Research Letters*, 2016, 11, Article n. 453.

[13] A. T. Mohamed, S. A. Ahmed, K. Ebnelwaled, A. Ahmed Ibrahim, "Improvement Optical and Electrical Characteristics of Thin Film Solar Cells Using Nanotechnology Techniques", *Intl. J. of Electronics and Telecom.*, 2019, vol. 65 (4), pp. 625-634, DOI: 10.24425/ijet.2019.129822.

[14] R. Rawat, R. Singh, O. S. Sastry, S. C. Kaushik, "Performance evaluation of micromorph based thin film photovoltaic modules in real operating conditions of composite climate", *Energy*, vol. 120, pp. 537-548, February 2017.

[15] W. M. Nkounga, M. F. Ndiaye, M. L. Ndiaye, O. Cisse, M. Bop, and A. Sioutas, "Short-term forecasting for solar irradiation based on the multi-layer neural network with the Levenberg-Marquardt algorithm and meteorological data: application to the Gandon site in Senegal,"*7th IEEE Int. Conf. on Ren. Energy Res. and Appl.*, Paris, October 2018, 869–874.

[16] J. Fan, L. Wu, F. Zhang, H. Cai, W. Zeng, X. Wang, H. Zou, "Empirical and machine learning models for predicting daily global solar radiation from sunshine duration: A review and case study in China," *Renewable and Sustainable Energy Reviews*, vol. 100, pp. 186–212, DOI: 10.1016/j.rser.2018.10.018, October 2018.

[17] M. U. Afzaal, I. Ali Sajjad, A. B. Awan, K. N. Paracha, M. F. N. Khan, A. R. Bhatti, M. Zubair, W. ur Rehman, S. Amin, S. S. Haroon, R. Liaqat, W. Hdidi and I. Tlili, "Probabilistic Generation Model of Solar Irradiance for Grid Connected Photovoltaic Systems Using Weibull Distribution," *Sustainability*, vol. 12, Article n. 2241; DOI: 10.3390/su12062241, March 2020.

[18] Y. Stauffer, D. Ferrario, E. Onillon, and A. Hutter, "Power monitoring based photovoltaic installation fault detection," *4th IEEE 2015 International Conference on Renewable Energy Research and Applications (ICRERA)*, Palermo, Italy, November 2015, 199–202.

[19] A. Bosio, A. Romeo, D. Menossi, S. Mazzamuto, and N. Romeo, "The second-generation of CdTe and CuInGaSe2 thin film PV modules," *Crystal Research and Technology*, vol. 46, pp. 857–864, October 2011.

[20] G. Acciari, A. Busacca, S. Guarino, A. Imburgia, A. Madonia, R. Miceli, A. Parisi, E. Riva Sanseverino, P. Romano, G. Sauba, G. Schettino, C. Spataro, F. Viola; "PV systems in the vertical walls: A comparison of innovative structures," *6th IEEE Int. Conference on Renewable Energy Research and Applications*, Birmingham, November 2016, 1185–1190.

[21] K.H. Ong, R. Agileswari, B. Maniscalco, P. Arnou, C. Chandan Kumar, J. W. Bowers, M. Bte Marsadek, "Review on Substrate and Molybdenum Back Contact in CIGS Thin Film Solar Cell," *Int. Journal of Photoenergy*, vol. 2018, pp. 1–14, September 2018.

[22] L. Chaar, "Solar Power Conversion," in Power Electronics Handbook (Second Edition), M. H. Rashid, Ed. Burlington: Academic Press, 2007, pp. 661–672.

[23] W. A. Badawy, "A review on solar cells from Si-single crystals to porous materials and quantum dots," *Journal of Advanced Research*, vol. 6, pp. 123–132, March 2015.

[24] S. Ananthakumar, J. Ram Kumar, S. Moorthy Babu, "Third-Generation Solar Cells: Concept, Materials Performance, an Overview," *Emerging Nanostructured Materials for Energy and Environmental Science*, pp. 305–339, February 2019.

[25] J. Yan and B. R. Saunders, "Third-generation solar cells: a review and comparison of polymer:fullerene, hybrid polymer and perovskite solar cells," *RSC Advances*, vol. 4, pp. 43286–43314, July 2014.

[26] P. V. Kamat, "Quantum Dot Solar Cells. The Next Big Thing in Photovoltaics," *Journal of Physics and Chemestry Letters*, vol. 4, pp. 908–918, February 2013.

[27] S. Il Cho, H. K. Sung, S.-Ju Lee, W. H. Kim, D.-H. Kim, Y. S. Han, "Photovoltaic Performance of Dye-Sensitized Solar Cells Containing ZnO Microrods," *Nanomaterials MDPI*, vol. 9, Article n. 1645, DOI:10.3390/nano9121645, November 2019.

[28] P. Tonui, S. O. Oseni, G. Sharma, Q. Yan, and G. Tessema Mola, "Perovskites photovoltaic solar cells: An overview of current status," *Renewable and Sustainable Energy Reviews*, vol. 91, pp. 1025–1044, June 2018.

[29] M. Yamaguchi, T. Takamoto, K. Araki, "Super high-efficiency multi-junction and concentrator solar cells," *Solar Energy Materials and Solar Cells*, vol. 90, no. 18-19, pp. 3068-3077, November 2006.

[30] P. Sánchez-Friera, M. Piliougine, J. Peláez, J. Carretero, M. Sidrach de Cardona, "Analysis of degradation mechanisms of crystalline silicon PV modules after 12 years of operation in Southern Europe," *Progress in Photovoltaics: Research and Applications*, vol. 19 pp. 658–666, January 2011.

[31] J. H. Wohlgemuth, D. Cunningham, P. Monus, J. Miller, A. Nguyen, "Long Term Reliability of Photovoltaic Modules," *4th IEEE World Conf. on Photovoltaic Energy*, Waikoloa, USA, pp. 2050–2053, May 2006.

[32] K. Morita, T. Inoue, H. Kato, I. Tsuda, Y. Hishikawa, "Degradation factor analysis of crystalline-Si PV modules through long-term field exposure test," *3rd IEEE Conf. on Photovoltaic Energy Conversion*, Osaka, pp. 1948-1951, May 2003.

[33] A. M. A. M. Serag ElDin, A. K. Abel-Rahman, A. H. H. Ali, and S. Ookawara; "Effect of dust deposition on performance of thin film photovoltaic module in harsh humid climate," in *2nd IEEE 2013 International Conference on Renewable Energy Research and Applications (ICRERA)*, Madrid, October 2013, 674–679, DOI**:** 10.1109/ICRERA.2013.6749839.

[34] A. Lay-Ekuakille, A. Ciaccioli, G. Griffo, P. Visconti, G. Andria; "Effects of Dust on Photovoltaic Measurements: A Comparative Study"; *Measurement*, vol. 113, pp. 181-188, June 2017.

[35] J. J. Vega Díaz, M. Vlaminck, D. Lefkaditis, S. A. Orjuela Vargas, H. Luong "Solar Panel Detection within Complex Backgrounds Using Thermal Images Acquired by UAVs," *Sensors MDPI*, vol. 20, Article n. 6219; DOI: 10.3390/s20216219, October 2020.

[36] C. Dunderdale, W. Brettenny, C. Clohessy, E. E. van Dyk, "Photovoltaic defect classification through thermal infrared imaging using a machine learning approach," *Progress in Photovoltaics: Research and Applications*, vol. 28, Issue 3, pp. 177 - 188, December 2019.

[37] S. Yadir, R. Bendaoud, A. EL-Abidi, H. Amiry, M. Benhmida, S. Bounouar, B. Zohal, H. Bousseta, A. Zrhaiba, A. Elhassnaoui, "Evolution of the physical parameters of photovoltaic generators as a function of temperature and irradiance: New method of prediction based on the manufacturer's datasheet," *Energy Conversion and Management*, vol. 203, Article n. 112141, January 2020.

[38] T. Shimizu, "Staebler-Wronski Effect in Hydrogenated Amorphous Silicon and Related Alloy Films," *Jpn. J. Appl. Phys.*, vol. 43, no. 6R, pp. 3257-3268, June 2004.

[39] M. Nardone and D. S. Albin, "Degradation of CdTe Solar Cells: Simulation and Experiment," *IEEE Journal of Photovoltaics*, vol. 5, pp. 962–967, May 2015.

[40] C. R. Corwine, A.O. Pudov, M. Gloeckler, S.H. Demtsu, J. R. Sites, "Copper inclusion and migration from the back contact in CdTe solar cells," *Solar En. Materials and Solar Cells*, vol. 82, pp. 481–489, May 2004.

[41] K. K. Chin, T. A. Gessert, Su-Huai Wei, "The roles of CU impurity states in CdTe thin film solar cells," *35th IEEE Phot. Specialists Conference*, Honolulu, HI, USA, pp. 1915–1918, 20-25 June 2010.

[42] K. Vamsi Krishna, V. Dutta, and P. D. Paulson, "Effect of electric field on spray deposited CdTe thin films," *Thin Solid Films*, vol. 444, pp. 17–22, November 2003.

[43] H. Zhao, A. Farah, D. Morel, and C. S. Ferekides, "The effect of impurities on the doping and VOC of CdTe/CdS thin film solar cells," *Thin Solid Films*, vol. 517, pp. 2365–2369, February 2009.

[44] J. Liu; S. Johnston; S. P. Harvey; D. Albin; P. Hacke, M. Al-Jassim, "Transmission Electron Microscopy Study on Degradation Mechanism of CdTe Thin-Film Solar Cells," in *2018 IEEE 7th Conf. on Photovoltaic Energy Conv.*, Waikoloa, Jun. 2018, pp. 3281–3284, DOI: 10.1109/PVSC.2018.8548094.

[45] D. J. Coyle, "Life prediction for CIGS solar modules part 1: modeling moisture ingress and degradation," *Progress in Photovoltaics: Research and Applications*, vol. 21, pp. 156–172, June 2013.

[46] M. E. Stuckelberger, T. Nietzold, B. West, R. Farshchi, D. Poplavskyy, J. Bailey, B. Lai, J. M Maser, M. I Bertoni, "Defect activation and annihilation in CIGS solar cells: an operando x-ray microscopy study," *J. Phys. Energy*, vol. 2, no. 2, pp. 1-14, February 2020, DOI: 10.1088/2515-7655/ab5fa6.

[47] M. Theelen, C. Foster, H. Steijvers, N. Barreau, Z. Vroon, M. Zeman, "The impact of atmospheric species on the degradation of CIGS solar cells," *Solar Energy Materials and Solar Cells*, vol. 141, pp. 49–56, October 2015, DOI: 10.1016/j.solmat.2015.05.019.

[48] M. Igalson, M. Wimbor, and J. Wennerberg, "The change of the electronic properties of CIGS devices induced by the 'damp heat' treatment," *Thin Solid Films*, vol. 403–404, pp. 320–324, February 2002.

[49] C. Yang, K. Song, X. L. Xu, G. Yao, Z.Y. Wu, "Strain dependent effect on power degradation of CIGS thin film solar cell," *Solar Energy*, vol. 195, pp.121-128, January 2020.

[50] M. Theelen, K. Bakker, H. Steijvers, S. Roest, P. Hielkema, N. Barreau, E. Haverkamp, "In Situ Monitoring of the Accelerated Performance Degradation of Solar Cells and Modules: A Case Study for Cu(In,Ga)Se2 Solar Cells," *J Vis Exp*, vol. 140, pp.1-10, October 2018.

[51] J. Kettle, V. Stoichkov, D. Kumar, M. Corazza, S. A.Gevorgyan, F. C. Krebs, "Using ISOS consensus test protocols for development of quantitative life test models in ageing of organic solar cells," *Solar Energy Mat. and Solar Cells*, vol. 167, pp. 53-59, August 2017.

[52] D. Angmo and F. C. Krebs, "Over 2 Years of Outdoor Operational and Storage Stability of ITO-Free, Fully Roll-to-Roll Fabricated Polymer Solar Cell Modules," *Energy Technology*, vol. 3, pp. 774–783, June 2015.

[53] K. Kawano, R. Pacios, D. Poplavskyy, J. Nelson, D. D.C. Bradley and J. R. Durrant, "Degradation of organic solar cells due to air exposure", *Solar Energy Materials and Solar Cells*, vol. 90, pp. 3520-3530, December 2006.

[54] S. Schafer, A. Petersen, T. A. Wagner, R. Kniprath, D. Lingenfelser, A. Zen, T. Kirchartz, B. Zimmermann, Uli Würfel, X. Feng, T. Mayer, "Influence of the indium tin oxide/organic interface on open-circuit voltage, recombination, and cell degradation in organic small-molecule solar cells," *Physical Review B*, vol. 83, pp. 1-12, April 2011.

[55] M. Azzouzi, "A study of the degradation of organic solar cells," Univ. Pol. de Catalunya, Barcellona, 2015. Available online: https://core.ac.uk/download/pdf/46605844.pdf (accessed on 23 February 2021).

[56] S. Savagatrup, A. D. Printz, T. F. O'Connor, A. V. Zaretski, D. Rodriquez, E. J. Sawyer, K. M. Rajan, R. I. Acosta, S. E. Root, D. J. Lipomi, "Mechanical degradation and stability of organic solar cells: molecular and microstructural determinants," *Energy*

Environ. Sci., vol. 8, pp. 55–80, Dec. 2014, doi: 10.1039/C4EE02657H.

[57] N.Kato, Y. Takeda, K. Higuchi, A. Takeichi, E. Sudo, H. Tanaka, T. Motohiro, T. Sano, T. Toyoda, "Degradation analysis of dye-sensitized solar cell module after long-term stability test under outdoor working condition," *Solar Energy Mat. and Solar Cells*, vol. 93, pp. 893–897, Jun. 2009.

[58] L. Ciani, M. Catelani, E. A. Carnevale; L. Donati M. Bruzzi, "Evaluation of the Aging Process of Dye-Sensitized Solar Cells Under Different Stress Conditions," *IEEE Trans. on Instrum. and Measurement*,vol. 64, pp. 1179–1187, May 2015.

[59] M.-E. Yeoh, A. Jaloman, K.Y. Chan, "Aging effect in dye-sensitized solar cells sealed with thermoplastic films," *Microelec. Int.*, vol. 36 (Issue 2), pp. 68–72, Jan. 2019.

[60] F. Kabir, S. N. Sakib, S. S. Uddin, "Effect of MWCNT's concentration in TiO2 based DSSC and degradation study of the cell," *J. of Ren. and Sustainable Energy*, vol. 11, pp. 1–15, Mar. 2019, DOI: 10.1063/1.5055725.

[61] Z. Song, A. Abate, S. C. Watthage, G. K. Liyanage, A. B. Phillips, U.Steiner; M.Graetzel, M. J. Heben, "In-situ observation of moisture-induced degradation of perovskite solar cells using laser-beam induced current," *43rd IEEE Photovoltaic Specialists Conf.*, Portland, OR, USA, pp. 1202–1206, June 2016.

[62] S. Zhang and G. Han, "Intrinsic and environmental stability issues of perovskite photovoltaics," *Progress in Energy*, vol. 2, pp. 1-44, May 2020.

[63] N. Aristidou, C. Eames, I. Sanchez-Molina, X. Bu, J. Kosco, M. Saiful Islam, S. A. Haque, "Fast oxygen diffusion and iodide defects mediate oxygen-induced degradation of perovskite solar cells," *Nature Comm.*, vol. 8, pp. 1-10, May 2017.

[64] S. G. Motti, D.Meggiolaro, A.J. Barker, E. Mosconi, C. A. R. Perini, J.M. Ball, M.G.M. Kim, F. De Angelis and A. Petrozza, "Controlling competing photochemical reactions stabilizes perovskite solar cells," *Nature Photonics*, vol. 13, pp. 532-540, August 2019.

[65] M. Saliba, M. Stolterfoht, C. M. Wolff, D. Neher, and A. Abate, "Measuring Aging Stability of Perovskite Solar Cells," *Joule*, vol. 2, no. 6, pp. 1019–1024, Jun. 2018, DOI: 10.1016/j.joule.2018.05.005.

[66] A. Lay-Ekuakille, A. Arnesano, P. Vergallo, "Thin-film-based CdTe PV Module Characterization: Measurements and Energy Prediction Improvement", *Rev. of Scientific Instruments*, vol.84, pp.15114-15117, May 2013.

[67] P. Visconti, V. Diviggiano, P. Primiceri, A. Lay-Ekuakille, "Experimental setup for calibration and optimized operation of Maximum Power Point Tracker applied to an innovative under-test photovoltaic system", *16th IEEE Int. Conf. on Environment and Electrical Engineering*, Florence, pp. 1-6, 7-10 June 2016.

[68] P. Visconti, A. Lay-Ekuakille, P. Primiceri, G. Cavalera, "Wireless energy monitoring system of photovoltaic plants with smart anti-theft solution integrated with control unit of household electrical consumption"; *Int. J. on Smart Sensing and Intelligent Systems*, vol. 9, pp. 681–708, June 2016.

[69] P. Visconti, R. Ria, G. Cavalera, "Development of smart PIC – based electronic equipment for managing and monitoring energy production of photovoltaic plan with wireless transmission unit", *J. of Engineering and Applied Sciences*, vol. 10, pp. 9434–9441, January 2015.

[70] D. Dirnberger, U. Kräling, H. Müllejans, E. Salis, K. Emery, Y Hishikawa, K Kiefer, "Progress in photovoltaic module calibration: results of a worldwide intercomparison between four reference laboratories", *Measurement Science and Technology*, vol. 25, pp. 1-18, July 2014.

[71] A. Guérin de Montgareuil, L. Sicot, J.-L. Martin, F. Mezzasalma, Y. Delesse, J. Merten, "A New Tool for the MotherPV Method: Modeling of the Irradiance Coefficient of Photovoltaic Modules," *24th European Photovoltaic Solar Energy Conference*, Hamburg, pp. 3305–3309, 21-25 Sep. 2009.

[72] K. Emery, "Calibration and Rating of Photovoltaics", *38th IEEE Photovoltaic Specialists Conference*, Austin, pp. 769-774 ,3–8 June 2012.

[73] D. Huang, M.A. Reshchikov, P. Visconti, F. Yun, H. Morkoc, J.Jasinski, Z. L.-Weber, C. Litton, "Comparative study of Ga and N- polar GaN films grown on sapphire substrates by molecular beam epitaxy" *J. Vacuum Science Tech. B*, vol. 20, pp. 2256-2264, Nov. 2002.

[74] Supsi, DACD-ISAAC MPPT3000 Datasheet V1.7, 2011. Available online: https://www.supsi.ch/isaac/servizi/fotovoltaico/mppt-3000_it.html, (accessed on 23 February 2021).

[75] P. Visconti, G. Cavalera "Intelligent System for Monitoring and Control of Photovoltaic Plants and for Optimization of Solar Energy Production", *15th Int. Conf. on Environment and Electrical Eng.*, Rome, pp. 1933–1938, 10-13 June 2015.

[76] M. Xiao, Z. Yu, and Y. Cui, "Evaluation and estimation of daily global solar radiation from the estimated direct and diffuse solar radiation," *Theoretical and Applied Climatology*, vol. 140, no. 3, pp. 983–992, May 2020.

[77] P. Visconti, R. de Fazio, P. Primiceri, D. Cafagna, N. I. Giannoccaro, "A solar-powered fertigation system based on low-cost wireless sensor network remotely controlled by farmer for irrigation cycles and crops growth optimization", *Intl. J. of Electronics and Telecom.*, vol. 66, pp. 59-68, April 2020.

[78] P. Visconti, P. Primiceri, G. Cavalera, "Wireless monitoring system of household electrical consumption with DALY-based control unit of lighting facilities remotely controlled by Internet"; *J. of Communications Software and Systems*, vol. 12, pp. 4 – 15, March 2016.

[79] MicroCal 20 - Multifunction Documenting Process Calibrator, 2007. Available online: http://www.eurotron.jp/img/pdf/08-40.3_e_microcal_20dpc_low.pdf, (accessed on 23 February 2021).

[80] E. Moshksar, T. Ghanbari, "Real-time estimation of solar irradiance and module temperature from maximum

power point condition", *IET Science, Measurement & Technology*", vol. 12, pp 807 – 815, October 2018.

[81] G. Xu, X. Huang, "Primary calibration of solar photovoltaic cells at the National Metrology centre of Singapore", *Energy Procedia*, vol. 25, pp. 70-75, December 2012.

[82] P. Visconti, P. Primiceri, C. Orlando, "Solar Powered Wireless Monitoring System of Environmental Conditions for Early Flood Prediction or Optimized Irrigation in Agriculture", *J. of Engineering and Applied Sciences*, vol. 11, pp. 4623 – 4632, November 2016.

[83] G. Mazurek, "Performance study of solar power source for wireless systems", *Intl. J. of Electronics and Telecom.*, vol. 59, pp. 271–276, September 2013.

[84] P. Visconti, C. Orlando, P. Primiceri; "Solar Powered WSN for monitoring environment and soil parameters by specific app for mobile devices usable for early flood prediction or water savings" *16th Int. Conf. on Environ. Electr. Eng.*, Florence, pp. 1-6, 7-10 June.

[85] K.A. Emery, C. R. Osterwald, "Solar cell efficiency measurements", *Solar Cells*, vol. 17, pp. 253-274, May 1986.

[86] R. de Fazio, D. Cafagna, G. Marcuccio, P. Visconti "Limitations and characterization of energy storage devices for harvesting applications", *Energies*, vol. 13, pp. 1-18, January 2020.

[87] J. Park, G. Bhat, A. Nk, C. S. Geyik, U. Y. Ogras, and H. G. Lee, "Energy per Operation Optimization for Energy-Harvesting Wearable IoT Devices," *Sensors*, vol. 20, no. 3, Art. no. 3, January 2020.

[88] E. Mendez, A. Ortiz , P. Ponce, I. Macias, D. Balderas, A. Molina, "Improved MPPT Algorithm for Photovoltaic Systems Based on the Earthquake Optimization Algorithm", *Energies*, vol. 13, pp. 1-24, March 2020.

[89] W. Hayder, E. Ogliari, A. Dolara, A. Abid, M. B. Hamed, L. Sbita, "Improved PSO: A Comparative Study in MPPT Algorithm for PV System Control under Partial Shading Conditions", *Energies*, vol. 13, pp. 1-22, March 2020.

[90] A. Bouaichi, A. A. Merrouni, C. Hajjaj, H. Zitouni, A. Ghennioui, A. El Amrani, C. Messaoudi, "In-situ inspection and measurement of degradation mechanisms for crystalline and thin film PV systems under harsh climatic conditions," *Energy Procedia*, vol. 157, pp. 1210–1219, Jan. 2019.

[91] M. Demirtaş, B. Tamyürek, E. Kurt, İ. Çetinbaş, M. K. Öztürk, "Effects of Aging and Environmental Factors on Performance of CdTe and CIS Thin-Film Photovoltaic Modules," *Journal of Elec Materi*, vol. 48, pp. 6890–6900, Nov. 2019, DOI: 10.1007/s11664-019-07172-z.

[92] A. Phinikarides, G. Makrides, B. Zinsser, M. Schubert, G. E. Georghiou, "Analysis of photovoltaic system performance time series: Seasonality and performance loss," *Renewable Energy*, vol. 77, pp. 51–63, May 2015, DOI: 10.1016/j.renene.2014.11.091.